Experimental Design for the Estimation of Photophysical Parameters of the Two-State Excited-State Proton-Exchange Reaction in the Presence of pH Buffer

Wenwu Qin, Nikola Basarić, and Noël Boens*

Department of Chemistry, Katholieke Universiteit Leuven, Celestijnenlaan 200F, 3001 Heverlee (Leuven), Belgium

Received: September 30, 2004; In Final Form: February 14, 2005

The excited-state proton-exchange reaction of commonly used fluorescent pH probes at physiological pH becomes reversible upon addition of pH buffer. Using computer-generated fluorescence decay surfaces, we investigated under which experimental conditions (pH, buffer concentration, and excitation and emission wavelengths) the rate constants describing the excited-state processes (k_{ij}) and the spectral parameters related to excitation ($\tilde{b}_1$) and emission ($\tilde{c}_1$) can be accurately and precisely estimated by global compartmental curve fitting. It was found that a minimum of three fluorescence decay traces should be collected for the pH probe in the presence of buffer. These three decays should be characterized by at least two different pH values and at least two different buffer concentrations. In addition to these three traces, a minimum of one trace corresponding to the pH probe without buffer has to be recorded. Furthermore, for the accurate estimation of k_{ij}, $\tilde{b}_1$, and $\tilde{c}_1$, at least two of these traces should be collected at the same pH and excitation and emission wavelengths. The experimental conditions should be chosen in such a way that decays with unambiguous biexponential character are obtained. For fluorescent pH probes with p$K_a \approx 7$ that are responsive in the near-neutral pH range, it is advisable to use buffers with pK_a^B values comparable to or higher than the pK_a of the probe. Because the changes in the decay times are already apparent with a small quantity of buffer, there is no need to use excessively high buffer concentrations. From a practical point of view, the best experimental design is attained when one combines in a single fluorescence decay surface traces originating from samples characterized by different pH values at the same buffer concentration with traces characterized by different buffer concentrations at the same pH and decays of samples without buffer measured at several pH values.

Introduction

Fluorescent pH indicators are widely used to investigate in vivo changes of proton concentrations *inside* living cells.[1] To measure pH quantitatively, it is crucial to match the pK_a of the indicator to the pH of the investigated system. The intracellular pH in the cytosol is close to neutral (generally between ~6.8 and 7.4), so fluorescent indicators with a pK_a of around 7 are required for cytosolic pH measurements. The most common fluorescent indicators for near-neutral pH measurements[1] (e.g., SNARF and SNAFL indicators[2,3] and BCECF[3,4]) are fluorescein- or rhodamine-type molecules. To understand the complex photophysics of fluorescein-derived pH indicators fully, it is essential to elucidate the excited-state dynamics of these molecular forms. Rate constants of excited-state processes and spectral parameters associated with excitation and emission are the key parameters to be determined.

The single-photon timing (or time-correlated single-photon counting) technique[5,6] provides time-resolved fluorescence data from which these parameters can be extracted. To identify the kinetic model for an excited-state process, a multidimensional fluorescence decay surface is measured under a variety of experimental conditions (pH, excitation and emission wavelengths, etc.). In many cases, the time relaxation of an excited system can be described by a sum of exponential functions, which are expressed in terms of decay times τ and the corresponding preexponential factors α. Accurate estimations of τ and α values can be realized by the global analysis approach where the decay times τ can be linked (e.g., over decay traces collected at various emission wavelengths).[7−9] However, for decays collected at various pH values, τ generally varies and hence cannot be linked. To benefit the most from the power of global analysis, one has to fit directly for the underlying parameters, namely, the rate constants and spectral parameters that can be linked indeed. This global compartmental analysis has the additional advantage that the parameters of interest are determined directly from the complete decay data surface in a single step.[10−13]

Deterministic identifiability deals with the determination of the parameters of a given model assuming error-free observations.[14−16] There are three possible outcomes to the deterministic identifiability analysis. (1) The parameters of an assumed model can be estimated uniquely, and the model is uniquely (globally) identifiable from the idealized experiment. (2) There are a finite number of alternative estimates for some or all of the model parameters that fit the data, and the model is locally identifiable. (3) An infinite number of model parameter estimates fit the data, and the model is unidentifiable from the experiment. Recently, we have studied the fluorescence kinetics and the *deterministic* identifiability of a model of the intermolecular two-state excited-state proton-exchange reaction and how the addition of pH buffer affects both.[17] In the absence of pH buffer, the model is unidentifiable. When a pH buffer is added to this photophysical

* To whom all correspondence should be addressed. E-mail: noel.boens@chem.kuleuven.ac.be.

10.1021/jp040645b CCC: $30.25
Published on Web 04/20/2005

SCHEME 1: Representation of the Kinetic Model of Ground and Excited-State Proton-Exchange Reactions in the Presence of pH Buffer[a]

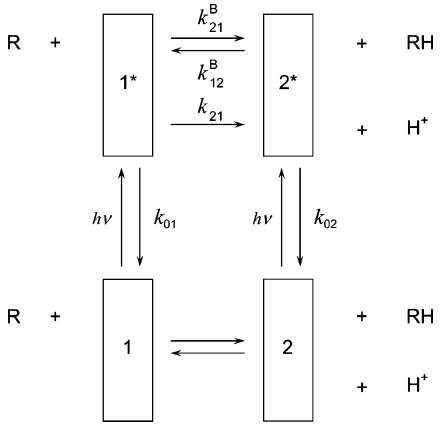

[a] **1** and **2** are, respectively, the ground-state acid and conjugate base forms of the fluorescent pH indicator, and **1*** and **2*** are the associated excited species. RH and R are, respectively, the acid and conjugate base forms of the buffer. In the time-resolved fluorescence experiments of fluorescein, RH is $H_2PO_4^-$, and R is HPO_4^{2-}.

system, the proton transfer becomes reversible, and the model is uniquely identifiable.

This paper describes the *numerical* identifiability of the model of the intermolecular two-state excited-state proton-exchange reaction. By using computer-generated noisy fluorescence decay traces that are in discrete (sampled) form, we verify the validity of the conclusions of the deterministic identification analysis. Hence, the problem comes down to estimating the parameters of the model (rate constants and spectral parameters related to absorption and emission) from experimental (here computer-generated) data by global compartmental curve fitting. This study allows one to determine the optimal experimental design of time-resolved fluorescence experiments of pH indicators so that the key parameters can be recovered with the highest accuracy.

Theory

Fluorescence Decay Kinetics. Consider a causal, linear, time-invariant intermolecular system consisting of two distinct types of ground-state species and two corresponding excited-state species as depicted in Scheme 1. Ground-state species **1** can deprotonate to form ground-state species **2** and H^+. The proton-exchange reaction is described by the ground-state acidity constant $K_a = [\mathbf{2}][H^+]/[\mathbf{1}]$ of the pH indicator. Photoexcitation creates excited-state species **1*** and **2***, which can decay by fluorescence (F) and nonradiative (NR) processes. The composite rate constants for these processes are denoted by k_{01} ($= k_{F1} + k_{NR1}$) and k_{02} ($= k_{F2} + k_{NR2}$). k_{21} denotes the rate constant for the dissociation of **1*** into **2*** and H^+. Because only pH probes useful at near-neutral pH will be considered in this paper, we will assume that $[H^+]$ is so small as to make the rate of association of $\mathbf{2}^* + H^+ \rightarrow \mathbf{1}^*$ negligible. The acidity of the buffer can be described by its ground-state acidity constant $K_a^B = [R][H^+]/[RH]$. In the ground state, the acidic form of the pH indicator (species **1**) can react with the basic form R of the pH buffer to give the basic form of the pH probe (species **2**) and the acidic form RH of the buffer. In the excited state, the reaction of species **1*** with R to form **2*** and RH is characterized by rate constant k_{21}^B. The reverse reaction of **2*** and RH to give **1*** and R is described by rate constant k_{12}^B.

If the system shown in Scheme 1 is excited with a δ pulse that does not significantly alter the concentrations of the ground-state species (i.e., in the low excitation limit), then the fluorescence δ-response function, $f(\lambda^{em}, \lambda^{ex}, t)$, at emission wavelength λ^{em} due to excitation at λ^{ex} is given by[12]

$$f(\lambda^{em}, \lambda^{ex}, t) = \kappa \tilde{\mathbf{c}}(\lambda^{em}) \mathbf{U} \exp(t\Gamma)\, \mathbf{U}^{-1} \tilde{\mathbf{b}}(\lambda^{ex}) \qquad t \geq 0 \tag{1}$$

with κ being a proportionality constant. $\mathbf{U} \equiv [\mathbf{U}_1, \mathbf{U}_2]$ is the matrix of the two eigenvectors of the compartmental matrix **A** (eq 2), and $\mathbf{U}^{-1}$ is the inverse of **U**. γ_1 and γ_2 are the eigenvalues of **A** corresponding to $\mathbf{U}_1$ and $\mathbf{U}_2$, respectively, and $\exp(t\,\Gamma) \equiv \mathrm{diag}[\exp(\gamma_1 t), \exp(\gamma_2 t)]$.

$$\mathbf{A} = \begin{bmatrix} -(k_{01} + k_{21} + k_{21}^B[R]) & k_{12}^B[RH] \\ k_{21} + k_{21}^B[R] & -(k_{02} + k_{12}^B[RH]) \end{bmatrix} \tag{2}$$

$\tilde{\mathbf{b}}(\lambda^{ex})$ is the 2×1 column vector with elements $\tilde{b}_i(\lambda^{ex})$ defined by

$$\tilde{b}_i = \frac{b_i}{b_1 + b_2} \tag{3}$$

where b_i denotes the concentration of i^* at time zero

$$b_i = [i^*]_{t=0} \tag{4}$$

which in the low-excitation limit is proportional to the ground-state absorbance of i. Hence, $\tilde{b}_i$ represents the normalized absorbance of species i at λ^{ex}. The $\tilde{\mathbf{b}}(\lambda^{ex}, \mathrm{pH})$ parameters can be expressed as a function of the ground-state acidity constant K_a of the pH indicator, the molar absorption coefficients $\epsilon_i(\lambda^{ex})$ of ground-state species i at λ^{ex}, and the pH of the sample solution. For $\tilde{b}_1(\lambda^{ex}, \mathrm{pH})$ at $[H^+]$ and λ^{ex}, we have

$$\tilde{b}_1(\lambda^{ex}, \mathrm{pH}) = \frac{[H^+]}{[H^+] + K_a \dfrac{\epsilon_2(\lambda^{ex})}{\epsilon_1(\lambda^{ex})}} \tag{5}$$

$\tilde{\mathbf{c}}(\lambda^{em})$ is the 1×2 row vector of the normalized emission weighting factors $\tilde{c}_i(\lambda^{em})$ of species i^* at λ^{em}:[12]

$$\tilde{c}_i = \frac{c_i}{c_1 + c_2} \tag{6}$$

The emission weighting factors $c_i(\lambda^{em})$ are given by[12]

$$c_i(\lambda^{em}) = k_{Fi} \int_{\Delta\lambda^{em}} \rho_i(\lambda^{em})\, \mathrm{d}\lambda^{em} \tag{7}$$

k_{Fi} represents the fluorescence rate constant of species i^*; $\rho_i(\lambda^{em})$ is the emission density of species i^* at emission wavelength λ^{em}, normalized to the complete steady-state fluorescence spectrum F_i of species i^*; and $\Delta\lambda^{em}$ is the emission wavelength interval around λ^{em} where the fluorescence signal is monitored. $\rho_i(\lambda^{em})$ is defined by[12]

$$\rho_i(\lambda^{em}) = \frac{F_i(\lambda^{em})}{\displaystyle\int_{\text{full band}} F_i\, \mathrm{d}\lambda^{em}} \tag{8}$$

Equation 1 can be written in the common biexponential format:

$$f(\lambda^{em}, \lambda^{ex}, t) = \alpha_1 \exp(\gamma_1 t) + \alpha_2 \exp(\gamma_2 t) \qquad t \geq 0 \tag{9}$$

The eigenvalues $\gamma_{1,2}$ are given by

$$\gamma_{1,2} = -\frac{1}{2}[(S_1 + S_2) \mp \sqrt{(S_1 - S_2)^2 + 4k_{12}^{B}[RH](k_{21} + k_{21}^{B}[R])}] \quad (10)$$

with

$$S_1 = k_{01} + k_{21} + k_{21}^{B}[R] \quad (11a)$$

$$S_2 = k_{02} + k_{12}^{B}[RH] \quad (11b)$$

and are related to the decay times $\tau_{1,2}$ according to

$$\gamma_{1,2} = -\frac{1}{\tau_{1,2}} \quad (12)$$

The exponential factors $\gamma_{1,2}$ (and hence also $\tau_{1,2}$) are dependent on pH because [R] and [RH] are generally pH-dependent. Indeed, [R] and [RH] can be expressed as a function of $[H^+]$, K_a^B of the buffer, and the analytical buffer concentration C^B (= [R] + [RH]):

$$[R] = \frac{K_a^B C^B}{K_a^B + [H^+]} \quad (13a)$$

$$[RH] = \frac{[H^+]C^B}{K_a^B + [H^+]} \quad (13b)$$

Preexponentials $\alpha_{1,2}$ are dependent on rate constants k_{ij}, pH, λ^{ex}, λ^{em}, and total buffer concentration C^B.[17]

When the pH is much higher than the pK_a and pK_a^B, only species **2** and **2*** are present, and [RH] $\approx$ 0 ($C^B \approx$ [R]). In that case, the value of amplitude α_1 associated with the limiting value of $\tau_1 = (k_{01} + k_{21} + k_{21}^{B}C^B)^{-1} = S_1^{-1}$ vanishes. Hence, the fluorescence δ-response function is given by eq 14

$$f(\lambda^{em}, \lambda^{ex}, t) = b_2 c_2 \exp(-k_{02}t) \qquad t \geq 0 \quad (14)$$

and this assigns a unique value to k_{02}.

Deterministic Identifiability. Recently, we completed a deterministic identifiability analysis of the model shown in Scheme 1.[17] At least three fluorescence decays collected at a minimum of two pH values and at a minimum of two buffer concentrations, in combination with the biexponential fluorescence decay in the absence of buffer (i.e., $C^B = 0$), are necessary and sufficient to uniquely determine all rate constants k_{ij} and normalized spectral parameters $\tilde{\mathbf{b}}$ and $\tilde{\mathbf{c}}$. The requirement is that the decays at the common pH should be collected under identical experimental conditions (λ^{ex} and λ^{em}). Figure 1 shows graphically the experimental configurations as a function of pH and C^B that lead to the unique determination of all rate constants k_{ij}. All four cases depend on the crucial measurement of a biexponential decay of the pH indicator at $C^B = 0$ so that the sum ($k_{01} + k_{21} + k_{02}$) is known.

Experimental Section

Synthetic Data Generation. Simulated fluorescence decay traces were generated by the convolution of $f(\lambda^{ex}, \lambda^{em}, t)$ with a synthetic instrument response function consisting of a difference of two exponentials. The full width at half-maximum of the instrument response function is ~60 ps. Preexponential factors $\alpha_{1,2}$ and corresponding eigenvalues $\gamma_{1,2}$ were computed from k_{ij}, $\tilde{b}_1$, and $\tilde{c}_1$ by a dedicated computer program using the

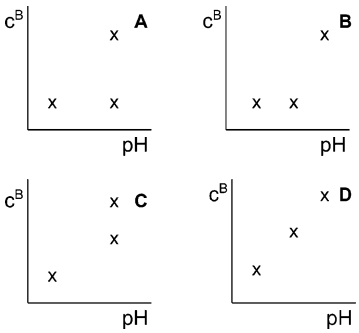

Figure 1. Possible experimental configurations as a function of pH and buffer concentration C^B that lead to uniquely determined rate constants. All four cases depend on the knowledge of the sum ($k_{01} + k_{21} + k_{02}$), which can be obtained from a biexponential decay without pH buffer ($C^B = 0$).

TABLE 1: Simulation Parameter Values Used for the Computation of Decay Times $\tau_{1,2}$ and the Associated Preexponential Factors $\alpha_{1,2}$ in the Presence of pH Buffer[a]

parameter	value
k_{01}	0.6×10^9 s^{-1}
k_{02}	0.8×10^9 s^{-1}
k_{21}	1×10^9 M^{-1} s^{-1}
k_{12}^B	(5 or 30) $\times 10^9$ M^{-1} s^{-1}
k_{21}^B	10×10^9 M^{-1} s^{-1}
pK_a	7.5
ϵ_1/ϵ_2	1

[a] The preexponentials are calculated for four detection wavelengths corresponding to the following $\tilde{c}_1$ values (0.6, 0.4, 0.2, and 0.0). The $\tilde{b}_1$ values are calculated according to eq 5.

(arbitrary) simulation parameter values given in Table 1 for four $\tilde{c}_1$ values (0.6, 0.4, 0.2, and 0.0). The rate constant values were chosen to obtain decay times $\tau_{1,2}$ in the (sub)nanosecond range commonly measured by the single-photon timing technique. The other parameter values were selected to produce significant changes in the decay times $\tau_{1,2}$ and preexponential factors $\alpha_{1,2}$ as a function of pH and C^B. The $\gamma_{1,2}$ and $\alpha_{1,2}$ values were then used to compute biexponential δ-response functions $f(\lambda^{ex}, \lambda^{em}, t)$ according to eqs 9−13. The scaling factor was adjusted to reach about 10^4 counts in the peak channel. All computer-generated decays had 4K data points. The time increment per channel was 2 or 3 ps. Full details of the synthetic fluorescence decay data generation are presented elsewhere.[18]

Implementation of Global Compartmental Analysis. The global compartmental curve fitting of the fluorescence decay surface of species undergoing excited-state processes in the presence of added buffer was implemented in a general global analysis program using Gaussian-weighted nonlinear least-squares fitting based on Marquardt−Levenberg minimization.[19] Any of the fitting parameters can be kept fixed during the fitting or may be freely adjustable to seek optimum values.

Consider the intermolecular two-state excited-state process in the presence of added buffer as represented in Scheme 1. The global (linkable) fitting parameters are k_{01}, k_{02}, k_{21}, k_{12}^B, k_{21}^B, $\tilde{b}_1$, and $\tilde{c}_1$. The rate constants k_{ij} can be linked over the whole decay surface, the $\tilde{b}_1$ parameters can be linked for samples at the same pH and λ^{ex}, and the $\tilde{c}_1$ parameters can be linked for samples at the same λ^{em}. The only local (nonlinkable) fitting parameters are the scaling factors.

At each pH and C^B, the values of [R] and [RH] of the buffer with acidity constant K_a^B were computed according to eq 13. Assigning initial guesses to rate constants k_{01}, k_{02}, k_{21}, k_{12}^B, and k_{21}^B allows one to construct the compartmental matrix **A** for

each decay trace. The starting value for all rate constants k_{ij} was 1×10^9 (M^{-1}) s^{-1}; for $\tilde{b}_1$ and $\tilde{c}_1$, the initial guesses were 0 and/or 1. For identifiable experimental configurations, the same final parameter estimates were obtained, regardless of the initial guesses of $\tilde{b}_1$ and $\tilde{c}_1$. Eigenvalues $\gamma_{1,2}$ and associated eigenvectors $\mathbf{U}_{1,2}$ of matrix **A** were determined using routines from EISPACK, Matrix Eigensystem Routines.[20] The eigenvectors were then scaled to the initial conditions $\tilde{b}$. The fluorescence δ response of the sample, $f(\lambda^{ex}, \lambda^{em}, t)$, was calculated according eq 1. Then $f(\lambda^{ex}, \lambda^{em}, t)$ was convoluted with the instrument response function, and the adjustable parameters of this calculated curve were optimized to fit the simulated (or experimental) fluorescence decay of the sample. The generalized global mapping table approach described previously[21] allows one to analyze simultaneously experiments done at different λ^{ex} and λ^{em}, at multiple timing calibrations, and at different pH and C^B values.

The fitting parameters were determined by minimizing the global *reduced* chi-square χ_g^2

$$\chi_g^2 = \sum_l^q \sum_i \frac{w_{li}(y_{li}^o - y_{li}^c)}{\nu} \qquad (15)$$

where the index l sums over q experiments and the index i sums over the appropriate channel limits for each individual experiment. y_{li}^o and y_{li}^c denote, respectively, the *o*bserved (experimental or synthetic) and *c*alculated (fitted) values corresponding to the ith channel of the lth experiment, and w_{li} is the corresponding statistical weight. ν represents the number of degrees of freedom for the entire multidimensional fluorescence decay surface. It is essential that all fitting parameters are subject to simple range constraints on their values. The problem of minimizing χ_g^2 can be stated mathematically as follows: minimize $\chi_g^2(x)$ for all x, $x \in R^n$ subject to $s_j \le x_j \le t_j$, with $j = 1, 2, ..., n$ and n being the number of adjustable parameters. This format assumes that lower and upper constraints exist on all fitting parameters. Restrictions on the values of a particular fitting parameter j can be removed by allowing very large negative and positive values of s_j and t_j, respectively. For all rate constants and local scaling factors, s_j was set at 0; the default constraints on $\tilde{b}_1$ and $\tilde{c}_1$ are $-0.2 \le \tilde{b}_1, \tilde{c}_1 \le 1.2$. Small, negative s_j values prevent oscillations in the nonlinear least-squares search that would occur if the values of the fitting parameters were forced to be nonnegative. These constraints can be adjusted, if necessary.

The statistical criteria used to judge the quality of the fit comprised both graphical and numerical tests. The graphical methods included plots of surfaces ("carpets") of the autocorrelation function values versus experiment number and of the weighted residuals versus channel number versus experiment number. The additional statistical criteria used to judge the quality of the fit are described elsewhere.[18]

Results and Discussion

Fluorescence Decay Kinetics. Many commonly used fluorescent pH indicators at physiological pH (around 7) and in the absence of added buffer can be described by Scheme 1. The proton concentration is very low (around 10^{-7} M) to make the bimolecular protonation reaction in the excited state negligible. Consequently, the decay times of excited species **1*** and **2*** are invariant with pH.[22] This is illustrated in Figure 2. When the fluorescence decay surface of such a system is analyzed via global compartmental curve fitting, it is impossible to determine

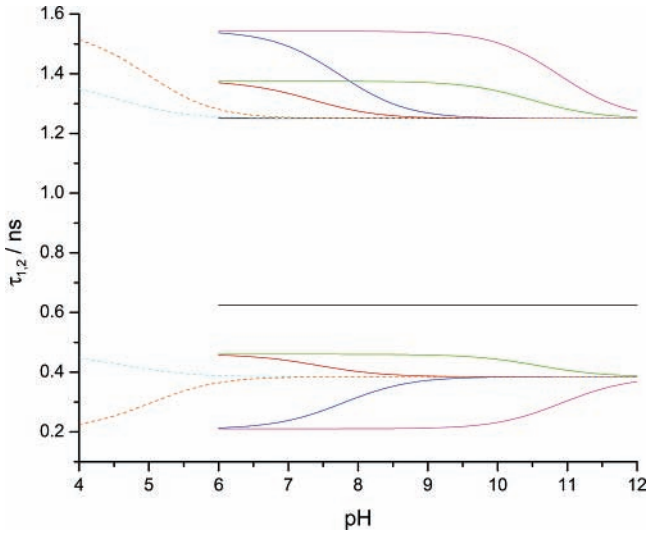

Figure 2. Dependence of $\tau_{1,2}$ on pH in the absence of buffer and at 0.1 M buffer characterized by different pK_a^B and k_{12}^B values. Black curves are without buffer, colors are with buffer (red, $pK_a^B = 7.5$ and $k_{12}^B = 5 \times 10^9$ M^{-1} s^{-1}; blue, $pK_a^B = 7.5$ and $k_{12}^B = 3 \times 10^{10}$ M^{-1} s^{-1}; green, $pK_a^B = 10.64$ and $k_{12}^B = 5 \times 10^9$ M^{-1} s^{-1}; violet, $pK_a^B = 10.64$ and $k_{12}^B = 3 \times 10^{10}$ M^{-1} s^{-1}; blue dashed, $pK_a^B = 4.74$ and $k_{12}^B = 5 \times 10^9$ M^{-1} s^{-1}; orange dashed, pK_a^B decay times corresponding to τ_1 and the longer ones corresponding to τ_2. For clarity, the $\tau_{1,2}$ values for buffers with $pK_a^B = 7.5$ and 10.64 are displayed only for pH $\ge$ 6.0. The simulation values of the other parameters are shown in Table 1.

individual values of rate constants k_{01} and k_{21}. Their sum ($k_{01} + k_{21}$) and the value of k_{02} are the only accessible parameters.[17] Increasing the proton concentration (i.e., lowering the pH) to a value that would influence the decay times of excited-species **1*** and **2*** is not an option for these pH indicators. Indeed, many interesting physiological phenomena take place near pH 7, and hence the pH indicator must be responsive (and be used) within this physiological pH range. Moreover, widely used commercial (e.g., fluorescein-based) pH indicators exhibit multiple pH-dependent ionic equilibria. At lower pH, equilibrium species other than those at physiological pH would be involved, so that the information obtained at low pH would not be relevant to physiological pH.

Upon addition of a pH buffer with a suitable pK_a^B, the decay times of excited-state species **1*** and **2*** become pH-dependent (because [R] and [RH] are pH-dependent, see eqs 10−13 and Figure 2). The largest change in $\tau_{1,2}$ is observed in the pH range around pK_a^B, where the change in [R] and [RH] is most pronounced. Simulation values of 4.74, 7.50, and 10.64 for pK_a^B were chosen to mimic acetate, HEPES, and butylamine buffers, respectively. The magnitude of the change depends on the values of rate constants k_{ij}. Note that the largest change in $\tau_{1,2}$ in the presence of a buffer characterized by $pK_a^B = 4.74$ is found in the pH region of 4−6, outside the physiological pH range. For the commonly used fluorescent pH probes with $pK_a \approx 7$ that are responsive in the near-neutral pH range, it is advisable to use buffers with pK_a^B values comparable to or higher than the pK_a of the probe. Indeed, in the useable pH region of probes with $pK_a \approx 7$, buffers with low pK_a^B ($\le$5) have practically no influence on $\tau_{1,2}$. As stated before, working under more acidic conditions is not an alternative because new species governed by other equilibria might appear at lower pH. It is evident from Figure 2 that all τ_2 values converge at high pH to the value of $1/k_{02}$ (eq 14). This, however, is not the case for the τ_1 values.

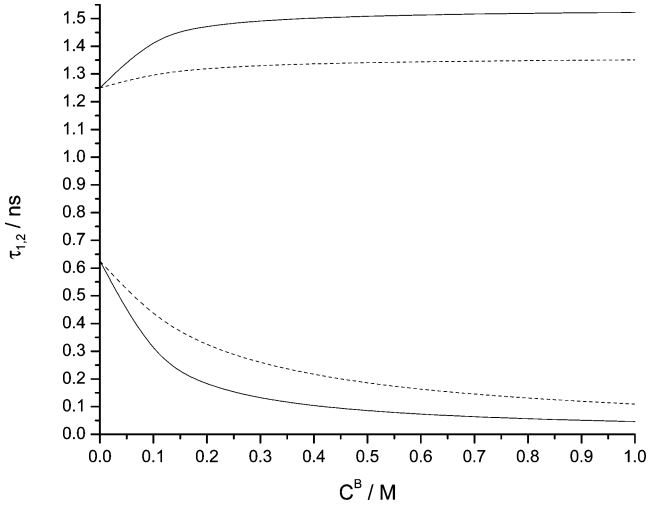

Figure 3. Dependence of $\tau_{1,2}$ on C^B and k_{12}^B ($pK_a^B = 7.5$; solid curve, $k_{12}^B = 3 \times 10^{10}$ M^{-1} s^{-1}; dashed curve, $k_{12}^B = 5 \times 10^9$ M^{-1} s^{-1}) at pH 7.5. The shorter decay times correspond to τ_1, and the longer ones correspond to τ_2. The simulation values of the other parameters are compiled in Table 1.

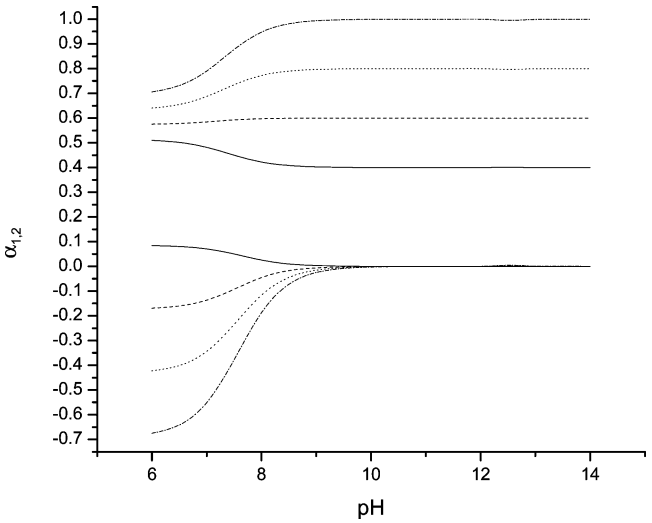

Figure 4. Dependence of $\alpha_{1,2}$ on pH in the presence of 0.1 M buffer ($pK_a^B = 7.5$, $k_{12}^B = 5 \times 10^9$ M^{-1} s^{-1}) corresponding to different $\tilde{c}_1$ values (solid curve, $\tilde{c}_1 = 0.6$; dashed curve, $\tilde{c}_1 = 0.4$; dotted curve, $\tilde{c}_1 = 0.2$; dashed−dotted curve, $\tilde{c}_1 = 0.0$). The upper curves correspond to α_2, and the lower ones correspond to α_1. The simulation values of the other parameters are compiled in Table 1.

The influence of the analytical buffer concentration C^B on the decay times $\tau_{1,2}$ is presented in Figure 3, where the calculated $\tau_{1,2}$ values are plotted in the presence of two buffers characterized by different k_{12}^B values. It is clear that the changes in $\tau_{1,2}$ are already apparent with a small quantity of buffer. Further increases in buffer concentration have a diminishing influence on $\tau_{1,2}$. In practical terms, this means that there is no need to use excessively high buffer concentrations that may introduce some other undesired phenomena such as problems of solubility, change in viscosity, and so forth.

In Figures 4 and 5, the dependence of preexponential factors $\alpha_{1,2}$ on pH, pK_a^B, and spectral parameter $\tilde{c}_1$ is presented. It is evident that $\alpha_{1,2}$ change in the region of pK_a and pK_a^B. Depending on the experimental conditions, decay curves could have more or less clear-cut biexponential character. At high enough pH, the decays become monoexponential ($\alpha_1 = 0$) with $\tau_2 = 1/k_{02}$ (eq 14). This very useful information allows one to determine which lifetime corresponds to which species.

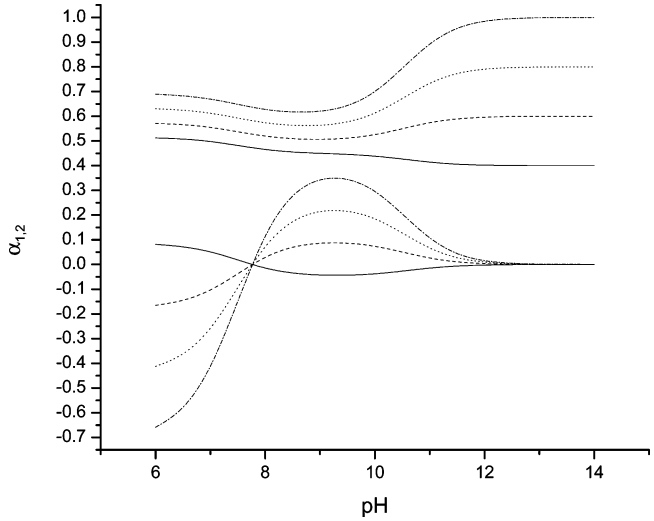

Figure 5. Dependence of $\alpha_{1,2}$ on pH in the presence of 0.1 M buffer ($pK_a^B = 10.64$, $k_{12}^B = 5 \times 10^9$ M^{-1} s^{-1}) corresponding to different $\tilde{c}_1$ values (solid curve, $\tilde{c}_1 = 0.6$; dashed curve, $\tilde{c}_1 = 0.4$; dotted curve, $\tilde{c}_1 = 0.2$; dashed−dotted curve, $\tilde{c}_1 = 0.0$). The upper curves correspond to α_2, and the lower ones correspond to α_1. The simulation values of the other parameters are compiled in Table 1.

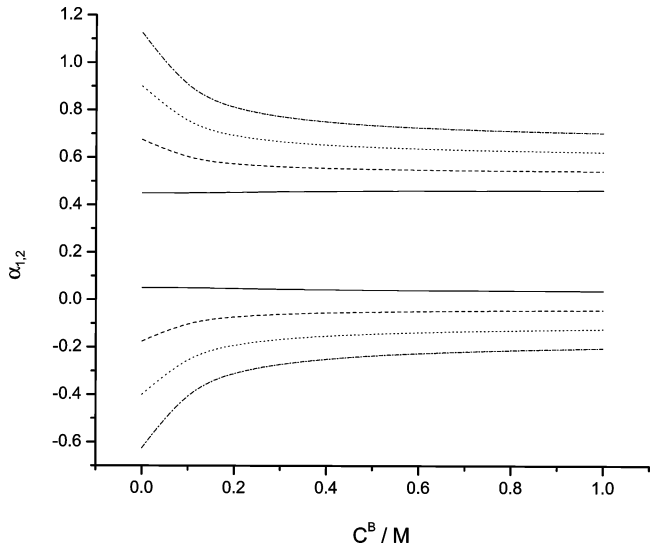

Figure 6. Dependence of $\alpha_{1,2}$ on C^B at pH 7.5 ($pK_a^B = 7.5$, $k_{12}^B = 5 \times 10^9$ M^{-1} s^{-1}) corresponding to different $\tilde{c}_1$ values (solid curve, $\tilde{c}_1 = 0.6$; dashed curve, $\tilde{c}_1 = 0.4$; dotted curve, $\tilde{c}_1 = 0.2$; dashed−dotted curve, $\tilde{c}_1 = 0.0$). The upper curves correspond to α_2, and the lower ones correspond to α_1. The simulation values of the other parameters are compiled in Table 1.

The influence of C^B on $\alpha_{1,2}$ at different $\tilde{c}_1$ values is presented in Figure 6. Again, as was the case for decay times $\tau_{1,2}$ (Figure 3), even a small concentration of buffer has a large influence on $\alpha_{1,2}$, but further increases in buffer concentration have only a limited extra effect. Once again, this eliminates the need to use very high buffer concentrations.

Curve Fitting of Simulated Decay Surfaces. In this section, we shall investigate how accurately and precisely the relevant model parameters (k_{ij}, $\tilde{b}_1$, and $\tilde{c}_1$) can be estimated by global compartmental curve fitting of computer-generated fluorescence decay surfaces. That way we can verify the validity of the conclusions of the *deterministic* identification analysis[17] and point the way to a rational experimental design (that involves how many decay traces have to be included in the analysis and under what experimental conditions they should be recorded).

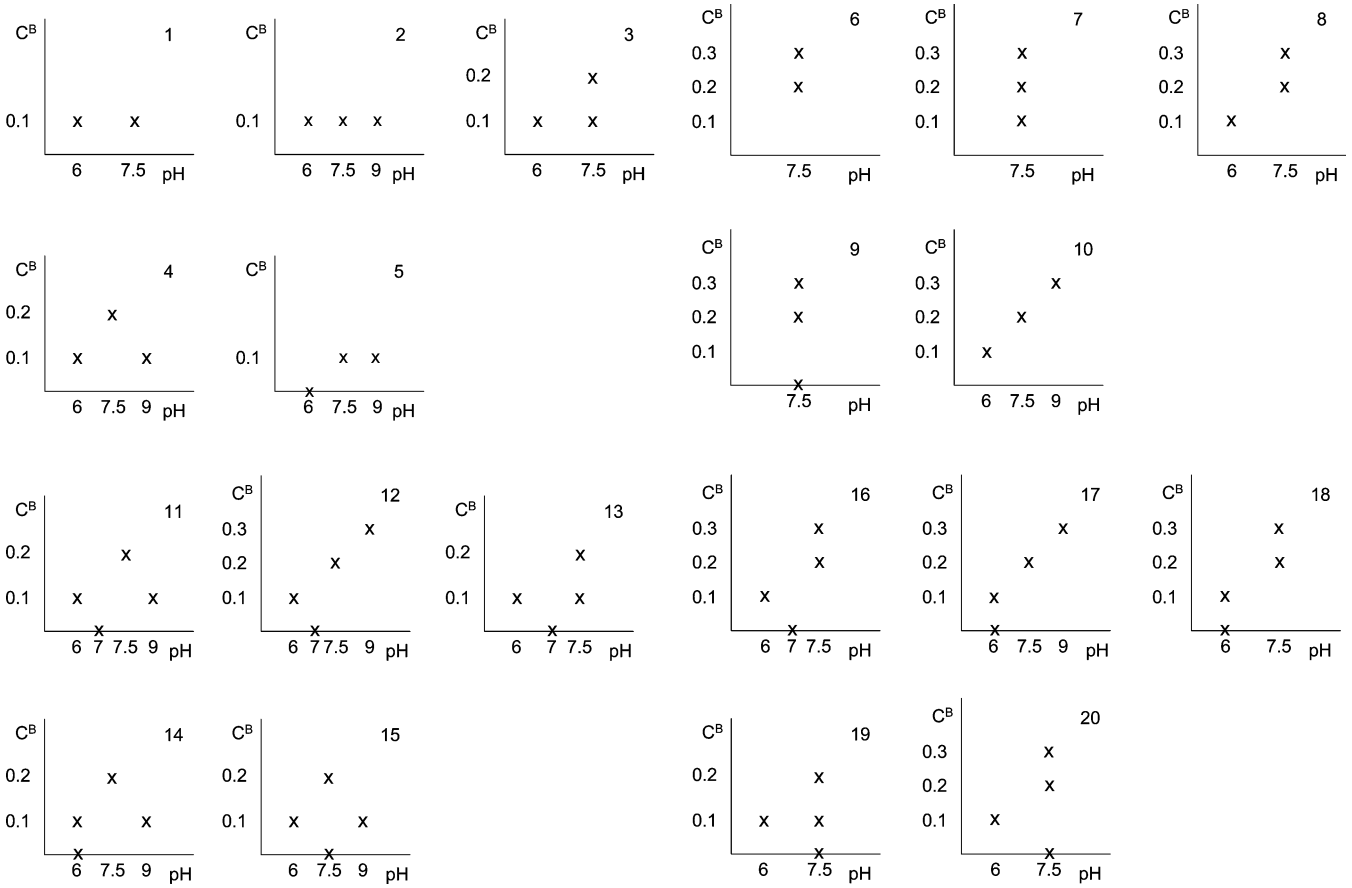

Figure 7. Experimental configurations with a minimum number (between two and four) of decay traces as a function of pH and C^B. For all experimental configurations, the time-resolved experiments are simulated at the same λ^{ex} and λ^{em}. The simulation values for the calculation of $\tau_{1,2}$ and $\alpha_{1,2}$ are compiled in Table 1. The buffer is assumed to be characterized by $pK_a^B = 7.5$. For all experimental configurations, we have $\tilde{c}_1 = 0.2$ and $k_{12}^B = 3 \times 10^{10}$ M^{-1} s^{-1}.

For the various experimental configurations depicted in Figure 7, computer-generated fluorescence decay surfaces were analyzed via global compartmental curve fitting. All experimental configurations depicted in Figure 7 have a minimal number of decay traces (between two and four), assuming that the same buffer was characterized by $pK_a^B = 7.5$ and $k_{12}^B = 3 \times 10^{10}$ M^{-1} s^{-1}, and were simulated at pH 6.0, 7.0, 7.5, and 9.0. In all configurations studied, the pK_a value of the fluorescent pH probe was taken to be 7.5, and the same wavelength of data collection was assumed, corresponding to $\tilde{c}_1 = 0.2$. All rate constants k_{ij} and the $\tilde{c}_1$ parameter were linked but kept freely adjustable in all curve fittings. The $\tilde{b}_1$ parameter was linked and adjustable at the same pH (and λ^{ex}). The simulation values of the other parameters are compiled in Table 1.

For reliable parameter estimation, it is essential that decays with an unambiguous biexponential nature are used and that the decay times vary considerably as a function of pH and C^B. When the decay traces of an experimental configuration that leads to a uniquely identifiable model are then analyzed via global compartmental curve fitting, it is expected that excellent fits will be obtained (χ_g^2 close to 1.0) and that the estimated parameters will closely match the simulation (true) values presented in Table 1. Fits resulting in inaccurate (and imprecise) parameter estimates then point to an experimental configuration that does not lead to unique identification.

Of the 20 configurations depicted in Figure 7, half of them are unidentifiable (giving wrong values for most or all k_{ij}, $\tilde{b}_1$, and $\tilde{c}_1$ values). Other configurations yield accurate estimates for k_{ij} but incorrect ones for $\tilde{b}_1$and $\tilde{c}_1$. Finally, some configurations are globally identifiable (in terms of k_{ij}, $\tilde{b}_1$, and $\tilde{c}_1$). Now let us look in detail at each configuration to see if we can elucidate the *numerical* results of the global compartmental curve fitting using the conclusions of the *deterministic* identifiability.[17]

When a fluorescence decay surface containing two curves (Figures 7-1) with the same C^B and different pH values was analyzed globally, a good fit was obtained, but all k_{ij}, $\tilde{b}_1$, and $\tilde{c}_1$ estimates were inaccurate. The incorrect estimates are to be expected on the basis of the results of the *deterministic* identifiability analysis.[17] Indeed, two pH values at a common C^B are insufficient to recover any reliable information. After the addition of a third curve at the same C^B but a different (higher) pH, resulting in the configuration of Figure 7-2, and global compartmental curve fitting of the resultant decay surface, a good fit to the three synthetic curves was obtained but with inaccurate parameter estimates, except for k_{02} (Table 2). At pH 9.0, the decay is nearly monoexponential (true $\alpha_1/\alpha_2 = 0.02$) with lifetime $\tau_2 = 1/k_{02}$, and this explains the accurate and precise k_{02} estimate. This is a general observation: the k_{02} value is estimated accurately (and precisely) whenever a decay trace at pH 9.0 is included in the global compartmental curve fitting. The configuration in Figure 7-3 also produces inaccurate estimates for all parameters, which is in perfect agreement with the conclusions of the deterministic identifiability. The configurations of Figure 7-4 and 7-5 yield similar results to the configuration in Figure 7-2: as anticipated, only k_{02} is accurately and precisely recovered (Table 2). For the configuration in Figure 7-5, one might expect accurate estimates for k_{12}^B and k_{21}^B,

TABLE 2: Parameters of the Configurations Depicted in Figure 7 Estimated by Global Compartmental Analysis[a]

	k_{01} (10^9 s^{-1})	k_{02} (10^9 s^{-1})	k_{21} (10^9 M^{-1} s^{-1})	k_{12}^B (10^9 M^{-1} s^{-1})	k_{21}^B (10^9 M^{-1} s^{-1})	$\tilde{b}_1$	$\tilde{c}_1$	χ_g^2
2	0.5 ± 0.1	0.799 ± 0.001	2.4 ± 0.9	17 ± 7	0.002 ± 7	0.006 0.274 0.736	0.167	1.028
5	0.1 ± 0.2	0.798 ± 0.001	1.5 ± 0.2	161 ± 122	1006 ± 806	0.003 0.073 1.009	0.299	1.026
11	0.601 ± 0.001	0.801 ± 0.002	0.992 ± 0.008	29.9 ± 0.7	9.9 ± 0.5	0.035 ± 43 0.535 ± 546 0.640 ± 1934 0.884 ± 1385	0.084 ± 2531	1.008
14	0.600 ± 0.001	0.801 ± 0.001	0.996 ± 0.006	29.6 ± 0.7	9.8 ± 0.5	0.031 ± 0.004 0.505 ± 0.005 0.965 ± 0.008	0.197 ± 0.004	1.014
17	0.600 ± 0.001	0.801 ± 0.001	0.996 ± 0.005	30.1 ± 0.7	10.2 ± 0.5	0.031 ± 0.009 0.498 ± 0.005 0.971 ± 0.009	0.201 ± 0.004	0.996
19	0.600 ± 0.002	0.803 ± 0.003	0.98 ± 0.02	29.9 ± 0.6	9.7 ± 0.5	0.508 ± 0.007 0.975 ± 0.009	0.203 ± 0.005	1.029
20	0.601 ± 0.001	0.803 ± 0.003	0.99 ± 0.02	30.1 ± 0.6	9.8 ± 0.4	0.507 ± 0.007 0.972 ± 0.009	0.200 ± 0.004	0.993

[a] The true (synthetic) k_{ij} values are compiled in Table 1. The true value of $\tilde{c}_1$ equals 0.2, whereas the true $\tilde{b}_1$ values at pH 6.0, 7.0, 7.5, and 9.0 are 0.97, 0.76, 0.5, and 0.03, respectively. The quoted errors are standard errors computed from the parameter covariance matrix available in the curve fitting.

but the almost monoexponential decay at pH 9.0 prevents that. Indeed, from the deterministic identification analysis it follows that two biexponential decays at the same nonzero C^B and two pH values combined with the knowledge of the sum ($k_{01} + k_{21} + k_{02}$) are sufficient to obtain unique solutions for k_{12}^B and k_{21}^B. A biexponential decay trace at $C^B = 0$ provides the required sum ($k_{01} + k_{21} + k_{02}$).

The configurations of Figure 7-6 (with two decay curves at the same pH and two nonzero C^B values) and of Figure 7-7 (with three decay curves at the same pH and three nonzero C^B values) have linked k_{ij}, $\tilde{b}_1$, and $\tilde{c}_1$. However, this does not guarantee unique identifiability. The inaccurate (and imprecise) values of k_{ij}, $\tilde{b}_1$, and $\tilde{c}_1$ recovered by global compartmental curve fitting confirm this. The same is true for the configurations depicted in Figure 7-8 to 7-10. For the analysis of the configuration in Figure 7-10, the value of k_{02} is estimated correctly. This is logical because a near-monoexponential decay at pH 9.0 was included in the decay surface.

A second group of configurations (Figure 7-11 and 7-12) yields unique and accurate values of k_{ij} only. The configuration in Figure 7-11 has two nonzero C^B values corresponding to three pH values and thus mimics the configuration depicted in Figure 1B. The configuration in Figure 7-12 has three nonzero C^B values corresponding to three pH values and thus matches the configuration depicted in Figure 1D. In both cases, an extra biexponential decay at $C^B = 0$ ensures that the sum ($k_{01} + k_{21} + k_{02}$) is known. According to the deterministic identifiability, these configurations should lead to unique values of k_{ij}. The global compartmental curve fittings of the four decay traces in Figure 7-11 and 7-12 confirm these findings. In both cases, inaccurate values of $\tilde{b}_1$ and $\tilde{c}_1$ were found (Table 2) because there is no linked $\tilde{b}_1$ parameter (no common pH).

The last group of configurations (Figure 7-13 to 7-20) leads to unique identifiability in terms of k_{ij}, $\tilde{b}_1$, and $\tilde{c}_1$. According to the deterministic identification analysis, all of these configurations should at least produce unique k_{ij} values. If there is a minimum of one common pH (as in all configurations in Figure 7-13 to 7-20), then the global compartmental curve fitting leads to the accurate estimation not only of k_{ij} but also of $\tilde{b}_1$ and $\tilde{c}_1$. The configurations of Figure 7-13 to 7-17 match the configurations of Figure 1A, B, B, C, and D, respectively. In all five cases, two decay traces have a common pH, and if these curves are recorded at the same excitation and emission wavelengths, then this produces, according to the deterministic identifiability analysis,[17] a quadratic equation in $\tilde{b}_1$ and $\tilde{c}_1$. If the same excitation wavelength is assumed at the common pH, then this reduces the number of estimable $\tilde{b}_1$ parameters in the curve fitting to three. Furthermore, in the simulations, a single $\tilde{c}_1$ value was assumed for the entire fluorescence decay surface. Thus, the number of spectral parameters that have to be determined is reduced to one linked $\tilde{c}_1$ and three $\tilde{b}_1$, and this leads to the accurate estimation of k_{ij}, $\tilde{b}_1$, and $\tilde{c}_1$. The configurations of Figure 7-18 to 7-20 match the configurations of Figure 1C, A, and C, respectively. In these configurations, two linked $\tilde{b}_1$ parameters and one linked $\tilde{c}_1$ have to be estimated by global compartmental curve fitting. The unique identifiability of the configurations in Figure 7-18 to 7-20 is shown in the accurate and precise values of k_{ij}, $\tilde{b}_1$, and $\tilde{c}_1$. Some representative examples of estimated parameters for the different experimental configurations presented in Figure 7 are shown in Table 2.

To study what information can be extracted by global compartmental curve fitting from the decay surface containing two decays at different pH values but a common nonzero C^B and one decay in the absence of buffer, the nine experimental configurations depicted in Figure 8 were simulated. They all have three simulated decay traces at pH 6.0, 7.5, and 9.0 and assumed the same buffer characterized by $pK_a^B = 7.5$ and $k_{12}^B = 3 \times 10^{10}$ M^{-1} s^{-1}. In all configurations studied, the pK_a value of the fluorescent pH probe was taken to be 7.5, and the same wavelength of data collection was assumed, corresponding to $\tilde{c}_1 = 0.2$. Rate constants k_{ij} and parameter $\tilde{c}_1$ were linked but kept freely adjustable in all parameter estimations. The simulation values of the other parameters are compiled in Table 1.

A knowledge of the sum ($k_{01} + k_{21} + k_{02}$) is a crucial requirement for having an identifiable model. A decay trace at $C^B = 0$ with clear biexponential character provides this information. However, at pH 9.0 the decays in the absence of buffer are practically monoexponential with a lifetime equal to $1/k_{02}$. This explains why the configurations of Figure 8-3, 8-6, 8-9 cannot be identified (Table 3). According to the deterministic

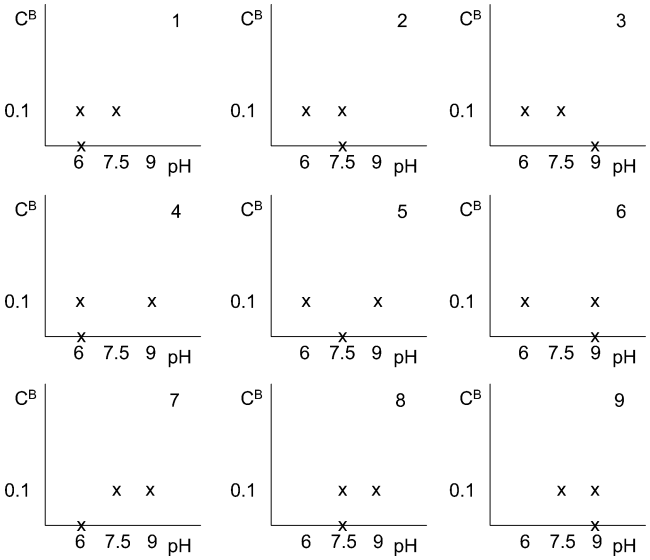

Figure 8. Experimental configurations with three decay traces as a function of pH and C^B. The other conditions are the same as in Figure 7.

identifiability,[17] rate constants k_{12}^B and k_{21}^B can be identified, whereas the solutions of the other rate constants are the roots of quadratic equations. The linked $\tilde{b}_1$ and $\tilde{c}_1$ parameters can be helpful in obtaining the correct rate constant values. Of the configurations of Figure 8, six configurations (8-1, 8-2, 8-4, 8-6, 8-8, 8-9) have a common pH (and hence linked $\tilde{b}_1$ in the curve fitting). Three (in Figure 8-1, 8-2, and 8-4) out of these six configurations indeed yield accurate and precise estimates for k_{ij}, $\tilde{b}_1$, and $\tilde{c}_1$ (Table 3). Although the decay trace in the absence of buffer at pH 7.5 in the configuration of Figure 8-8 is clearly biexponential, this configuration fails to give correct parameter estimates. The decays for 0.1 M buffer and pH 7.5 and 9.0 are close to monoexponential (true $\alpha_1/\alpha_2 = 0.02$), and this may be the reason that unacceptable parameter estimates are obtained. As found before (for the configurations of Figure 7-13 to 7-20), the constraint imposed by a $\tilde{b}_1$ parameter linked over several decays in the curve fitting (i.e., common to those decays) leads to the recovery of the true parameter values. Because $\tilde{b}_1$ is dependent on pH (eq 5), this further restricts the space of possible parameter estimates.

To test the influence of the (pK_a^B of the) buffer on identification, all of the experimental configurations of Figure 7 were duplicated with a buffer characterized by $pK_a^B = 10.64$ and $k_{12}^B = 3 \times 10^{10}$ M^{-1} s^{-1} at pH 6.0, 7.5, 10.5, and 12. The results obtained by global compartmental curve fitting of these experimental configurations were analogous to the results discussed above. This means that the pK_a^B value of the buffer does not influence the identifiability as long as the decays are noticeably biexponential and the decay times vary considerably as a function of pH and C^B. Of course, a change of the (pK_a^B of the) buffer changes the pH range where the decay times and preexponential factors vary. Therefore, the used pH range has to be modified to collect decay curves that are unmistakably biexponential.

In the previous sections, we have demonstrated what the requirements (with a minimum number of decay curves) are to achieve global identifiability. Under real experimental conditions, one generally wants to collect more decay traces than is strictly necessary for unique identifiability. Therefore, a fluorescence decay surface with a large number of curves is commonly measured as a function of λ^{ex}, λ^{em}, pH, and C^B to ensure unique identifiability and recover accurate (and precise) parameter estimates. Additionally, collecting decays at numerous excitation and emission wavelengths allows one to construct the species-associated excitation and emission spectra.[12] It is advantageous to collect traces at detection wavelengths where one form of the indicator's fluorescence predominates. Similarly, choosing λ^{ex} and/or pH where one ground-state form of the indicator is excited exclusively (or nearly so) might also be helpful in the data analysis.

Next we generated fluorescence decay surfaces consisting of many curves. It was assumed that the traces were collected at wavelengths corresponding to four $\tilde{c}_1$ values (0.6, 0.4, 0.2, and 0.0) in the absence and presence of buffer characterized by $pK_a^B = 10.64$ and $k_{12}^B = 5 \times 10^9$ M^{-1} s^{-1}. The simulation values of the other parameters are collected in Table 1.

TABLE 3: Parameters of the Configurations Depicted in Figure 8 Estimated by Global Compartmental Analysis[a]

	k_{01} (10^9 s^{-1})	k_{02} (10^9 s^{-1})	k_{21} (10^9 M^{-1} s^{-1})	k_{12}^B (10^9 M^{-1} s^{-1})	k_{21}^B (10^9 M^{-1} s^{-1})	$\tilde{b}_1$	$\tilde{c}_1$	χ_g^2
1	0.601 ± 0.001	0.801 ± 0.002	1.00 ± 0.01	30.0 ± 0.7	9.4 ± 0.7	0.967 0.500	0.198	1.022
2	0.601 ± 0.001	0.801 ± 0.003	0.99 ± 0.03	29.7 ± 0.8	9.4 ± 0.8	0.502 0.970	0.200	1.015
3	0.4 ± 0.2	0.795 ± 0.001	2.7 ± 0.8	16 ± 6	$4 \times 10^{-5} \pm 5$	−0.006 0.250 −0.008	0.734	1.008
4	0.600 ± 0.001	0.801 ± 0.002	0.99 ± 0.01	29.7 ± 0.8	7 ± 4	0.969 0.033	0.199	1.002
5	0.4 ± 0.2	0.795 ± 0.001	1.2 ± 0.2	16 ± 7	425 ± 215	1.009 0.051 0.611	0.346	1.034
6	$8 \times 10^{-5} \pm 1$	0.796 ± 0.001	2 ± 2	7 ± 11	431 ± 352	0.011 0.537	0.152	1.015
7	0.1 ± 0.2	0.798 ± 0.001	1.5 ± 0.2	161 ± 122	1007 ± 806	1.009 0.073 0.0033	0.299	1.026
8	0.5 ± 0.3	0.802 ± 0.003	1.1 ± 0.3	14 ± 17	4 ± 15	0.003 0.377	3×10^{-5}	1.007
9	0.66 ± 0.03	0.807 ± 0.008	0.6 ± 0.3	57 ± 29	10 ± 6	0.068 0.679	0.406	0.998

[a] The true (synthetic) k_{ij} values are compiled in Table 1. The true value of $\tilde{c}_1$ equals 0.2, whereas the true $\tilde{b}_1$ values at pH 6.0, 7.5, and 9.0 are 0.97, 0.5, and 0.03, respectively. The quoted errors are standard errors computed from the parameter covariance matrix available in the curve fitting.

TABLE 4: Parameters of Some Representative Experimental Configurations[a] Estimated by Global Compartmental Analysis[b]

	k_{01} (10^9 s^{-1})	k_{02} (10^9 s^{-1})	k_{21} (10^9 M^{-1} s^{-1})	k_{12}^B (10^9 M^{-1} s^{-1})	k_{21}^B (10^9 M^{-1} s^{-1})	$\tilde{c}_1$	number of curves	χ_g^2
1	0.0004 ± 0.3	0.801 ± 0.001	2.0 ± 0.3	1.3 ± 0.4	4.2 ± 0.6	0.444 0.746 0.838 0.882	36	1.023
2	0.4 ± 0.1	0.800 ± 0.001	1.5 ± 0.2	2.3 ± 0.5	9.3 ± 0.7	0.042 0.278 0.463 0.615	52	1.025
3	0.601 ± 0.001	0.802 ± 0.001	0.995 ± 0.003	4.98 ± 0.03	9.8 ± 0.4	0.001 0.200 0.399 0.600	80	1.023
4	0.60 ± 0.01	0.802 ± 0.001	1.00 ± 0.01	5.0 ± 0.3	24 ± 375	0.000 0.199 0.399 0.599	28	1.013
5	0.602 ± 0.001	0.801 ± 0.001	0.993 ± 0.003	5.03 ± 0.03	10.01 ± 0.06	0.007 0.203 0.400 0.600	116	1.017

[a] See the text. [b] The buffer is assumed to be described by $pK_a^B = 10.64$. The simulated configurations have $\tilde{c}_1 = 0.0$, 0.2, 0.4, and 0.6 and $k_{12}^B = 5 \times 10^9$ M^{-1} s^{-1}. The other simulation values are shown in Table 1. The quoted errors are standard errors computed from the parameter covariance matrix available in the curve fitting.

Via global compartmental curve fitting, the model was fitted to the synthetic fluorescence decay surfaces consisting of many curves corresponding to the same C^B (0.1 M) and different pH values. The fluorescence decay surfaces with 36 curves (at 4 $\tilde{c}_1$ values and 9 pH values between 8 and 12 in increments of 0.5 pH unit) and with 52 curves (also at 4 $\tilde{c}_1$ values and 13 pH values between 6 and 12 in increments of 0.5 pH unit) were analyzed via global compartmental curve fitting and yielded in both cases inaccurate and imprecise parameter estimates (entries 1 and 2 of Table 4). Predictably, the value of k_{02} could be estimated accurately and precisely because the decays at high pH (close to 12) are monoexponential with $\tau_2 = 1/k_{02}$. As shown above (Table 3, Figure 8), unique identification can be achieved when a minimal number of decay curves at the same (nonzero) C^B are analyzed in the presence of at least one curve without buffer at the same pH. Therefore, we added 28 curves at $C^B = 0$ (corresponding to the same 4 $\tilde{c}_1$ values and 7 equally spaced pH values between 6.0 and 9.0) to the fluorescence decay surface of 52 curves. The resulting fluorescence decay surface with 80 curves was then analyzed via global compartmental curve fitting, yielding unique, correct parameter estimates (entry 3 of Table 4).

To investigate whether many curves at the same pH (with pH $\ll pK_a^B$) but different C^B could lead to unique identifiability, we analyzed via global compartmental curve fitting a fluorescence decay surface with 20 curves [corresponding to five C^B values (0.1, 0.2, 0.3, 0.4, 0.5 M) and four $\tilde{c}_1$ values (0.6, 0.4, 0.2, 0.0)] at pH 7.5. The buffer was characterized by $pK_a^B = 10.64$ and $k_{12}^B = 5 \times 10^9$ M^{-1} s^{-1}. The simulation values of the other parameters are compiled in Table 1. A good global fit was obtained for this decay surface but with inaccurate (and imprecise) parameter estimates. When four curves corresponding to the same four $\tilde{c}_1$ values at $C^B = 0$ and at pH 7.5 were added to this surface, curve fitting of the resulting fluorescence decay surface did not produce unique identifiability. Adding to this fluorescence decay surface with 24 curves an extra 4 curves (with the same 4 $\tilde{c}_1$ values) without buffer and at pH 9.0 gave a good fit with accurate parameter estimates, except for k_{21}^B (entry 4 of Table 4). Deterministic identifiability[17] shows that when pH (7.5) $\ll pK_a^B$ (10.64), k_{12}^B can be determined at a single {pH, C^B} combination if the sum ($k_{01} + k_{21} + k_{02}$) is known. The biexponential decay at pH 7.5 and $C^B = 0$ yields the sum ($k_{01} + k_{21} + k_{02}$). If additionally ($k_{01} + k_{21}$) and k_{02} are separately known, then k_{01}, k_{21}, and k_{12}^B can be determined. This information is provided by decays in the absence of buffer at pH 7.5 and 9.0. For a buffer with $pK_a^B = 10.64$, most of the buffer is protonated ([RH] $\approx C^B$) at pH 7.5. Therefore, the reaction between R and **1*** is negligible, and this explains the inaccurate estimate of k_{21}^B with a large error (entry 4 of Table 4).

Finally, a computer-generated decay surface with 116 curves corresponding to 4 $\tilde{c}_1$ values (0.6, 0.4, 0.2, 0.0) and different pH and C^B values was created. Of the 116 curves, 52 corresponded to 13 equally spaced pH values between 6 and 12 at $C^B = 0.1$ M, 28 curves corresponded to 7 equally spaced pH values between 6.0 and 9.0 at zero buffer concentration, and 36 curves corresponded to 9 equally spaced buffer concentrations between 0.2 and 1 M at pH 10.5. Again the buffer was characterized by $pK_a^B = 10.64$ and $k_{12}^B = 5 \times 10^9$ M^{-1} s^{-1}. The simulation values of the other parameters are compiled in Table 1. Global compartmental curve fitting gave a unique solution with accurate and precise values of all estimated parameters (entry 5 of Table 4).

Conclusions

The excited-state reaction of many fluorescent pH probes used for measuring in vivo proton concentrations at physiological pH can be described as an irreversible excited-state proton-transfer reaction because proton concentrations at near-neutral pH are so low as to make the bimolecular protonation reaction negligible. The excited-state proton-exchange reaction becomes reversible upon addition of pH buffer. This results in the dependence of $\tau_{1,2}$ on pH and buffer concentration. The decay times $\tau_{1,2}$ change around pK_a^B, whereas the associated preexponentials $\alpha_{1,2}$ change in the region of pK_a^B and pK_a. For the widely used fluorescent pH probes with $pK_a \approx 7$ that are responsive in the near-neutral pH range, it is advisable to use buffers with pK_a^B values comparable to or higher than the pK_a of the probe to have a maximal effect on $\tau_{1,2}$ and $\alpha_{1,2}$. In the

useable pH region of probes with $pK_a \approx 7$, buffers with low pK_a^B (≤ 5) have practically no influence on $\tau_{1,2}$. Because the changes in $\tau_{1,2}$ are already apparent with a small quantity of buffer, there is no need to use excessively high buffer concentrations.

Using computer-generated decay traces, we have investigated under which experimental conditions (pH, C^B, λ^{ex}, and λ^{em}) the kinetic (rate constants k_{ij}) and spectral parameters ($\tilde{b}_1$ and $\tilde{c}_1$) defining the excited-state proton-exchange reaction in the presence of buffer can be accurately and precisely estimated by global compartmental curve fitting. The *numerical* results obtained by curve fitting agree superbly with the conclusions from the *deterministic* identifiability. A minimum of three fluorescence decay traces should be collected for the pH probe in the presence of buffer. These three decays should be characterized by at least two different pH values and at least two different nonzero buffer concentrations. In addition to these three traces, a minimum of one trace corresponding to the pH probe without buffer has to be recorded. Furthermore, to estimate k_{ij}, $\tilde{b}_1$, and $\tilde{c}_1$ accurately, at least two of these traces should be collected at the same pH, λ^{ex}, and λ^{em}. The experimental conditions should be chosen in such a way that decays with an unequivocally biexponential nature are obtained. In real experimental design, it is recommended that a higher number of curves than strictly necessary for unique identification be recorded and analyzed in a single step. Therefore, the best experimental design is realized when one combines in a single fluorescence decay surface traces originating from many samples defined by different pH values at the same C^B with traces characterized by a different C^B at the same pH and traces originating from samples without buffer measured if possible at the same pH as samples with buffer. All decay curves should preferably be collected at several emission wavelengths. Global compartmental curve fitting of such a decay surface by and large will yield accurate and precise estimates of k_{ij}, $\tilde{b}_1$, and $\tilde{c}_1$.

Acknowledgment. We are grateful to the University Research Fund of the Katholieke Universiteit Leuven for IDO-grant IDO/00/001 and postdoctoral fellowships to N.B. and W.Q. We thank the Fonds voor Wetenschappelijk Onderzoek − Vlaanderen for grant G.0320.00.

References and Notes

(1) Haugland, R. P. *Handbook of Fluorescent Probes and Research Products*, 9th ed.; Molecular Probes: Eugene, OR, 2002; p 827.
(2) Whitaker, J. E.; Haugland, R. P.; Prendergast, F. G. *Anal. Biochem.* **1991**, *194*, 330.
(3) Szmacinski, H.; Lakowicz, J. R. *Anal. Chem.* **1993**, *65*, 1668.
(4) Rink, T. J.; Tsien, R. Y.; Pozzan, T. *J. Cell. Biol.* **1982**, *95*, 189−196.
(5) O'Connor, D. V.; Phillips, D. *Time-Correlated Single Photon Counting*; Academic Press: London, 1984.
(6) Boens, N. In *Luminescence Techniques in Chemical and Biochemical Analysis*; Baeyens, W. R. G., De Keukeleire, D., Korkidis, K., Eds.; Marcel Dekker: New York, 1991; p 21.
(7) Knutson, J. R.; Beechem, J. M.; Brand, L. *Chem. Phys. Lett.* **1983**, *102*, 501.
(8) Beechem, J. M.; Brand, L. *Photochem. Photobiol.* **1986**, *44*, 323.
(9) Janssens, L. D.; Boens, N.; Ameloot, M.; De Schryver, F. C. *J. Phys. Chem.* **1990**, *94*, 3564.
(10) Beechem, J. M.; Ameloot, M.; Brand, L. *Chem. Phys. Lett.* **1985**, *120*, 466.
(11) Ameloot, M.; Beechem, J. M.; Brand, L. *Chem. Phys. Lett.* **1986**, *129*, 211.
(12) Ameloot, M.; Boens, N.; Andriessen, R.; Van den Bergh, V.; De Schryver, F. C. *J. Phys. Chem.* **1991**, *95*, 2041.
(13) Andriessen, R.; Boens, N.; Ameloot, M.; De Schryver, F. C. *J. Phys. Chem.* **1991**, *95*, 2047.
(14) Jacquez, J. A. *Compartmental Analysis in Biology and Medicine*; Elsevier: Amsterdam, 1972.
(15) Godfrey, K. *Compartmental Models and Their Application*; Academic Press: London, 1983.
(16) Anderson, D. H. *Compartmental Modeling and Tracer Kinetics*; Lecture Notes in Biomathematics; Springer-Verlag: Berlin, 1983; Vol. 50.
(17) Boens, N.; Basarić, N.; Novikov, E.; Crovetto, L.; Orte, A.; Talavera, E. M.; Alvarez-Pez, J. M. *J. Phys. Chem. A* **2004**, *108*, 8180.
(18) Van den Zegel, M.; Boens, N.; Daems, D.; De Schryver, F. C. *Chem. Phys.* **1986**, *101*, 311.
(19) Program developed jointly by the Technology Institute of the Belarusian State University (Minsk, Belarus) and the Division of Photochemistry and Spectroscopy of Katholieke Universiteit Leuven, Leuven, Belgium.
(20) Smith, B. T.; Boyle, J. M.; Garbow, B. S.; Ikeke, Y.; Klema, V. C.; Moler, C. B. In *Lecture Notes in Computer Science*; Goos, G., Hartmanis, J., Eds.; Springer-Verlag: Heidelberg, Germany, 1974; Vol. 6.
(21) Boens, N.; Janssens, L. D.; De Schryver, F. C. *Biophys. Chem.* **1989**, *33*, 77.
(22) Boens, N.; Kowalczyk, A.; Cielen, E. *J. Phys. Chem.* **1996**, *100*, 4879.